Prediction of the Bottomonium D-Wave Spectrum from Full Lattice QCD

J. O. Daldrop,* C. T. H. Davies,† and R. J. Dowdall‡

(HPQCD Collaboration)§

SUPA, School of Physics and Astronomy, University of Glasgow, Glasgow, G12 8QQ, United Kingdom
(Received 12 December 2011; published 8 March 2012)

We calculate the full spectrum of D-wave states in the Υ system in lattice QCD for the first time, by using an improved version of nonrelativistic QCD on coarse and fine ''second-generation'' gluon field configurations from the MILC Collaboration that include the effect of up, down, strange, and charm quarks in the sea. By taking the $2S$-$1S$ splitting to set the lattice spacing, we determine the $^3D_2$-$1\bar{S}$ splitting to 2.3% and find agreement with experiment. Our prediction of the fine structure relative to the $^3D_2$ gives the $^3D_3$ at 10.181(5) GeV and the $^3D_1$ at 10.147(6) GeV. We also discuss the overlap of $^3D_1$ operators with $^3S_1$ states.

DOI: 10.1103/PhysRevLett.108.102003 PACS numbers: 12.38.Gc, 11.15.Ha, 14.40.Nd, 14.40.Pq

Introduction.—The spectrum of $b\bar{b}$ states has provided a very important testing ground for strong interaction physics because of the number of radial and orbital excitations that are ''gold-plated,'' i.e., well below the threshold for decay to B mesons. The recent discovery of the $\eta_b(1S)$ [1] and $h_b(1P)$ and $h_b(2P)$ mesons [2] filled in important gaps in the spin-singlet states. The mass of the η_b meson had previously been predicted by lattice QCD [3], and the h_b meson masses were widely expected, and found, to be very close to the spin average of their associated spin-triplet states.

The key missing gold-plated mesons are now the $\Upsilon(1D)$ states. These are very difficult to find experimentally, although the $^3D_2$ has been seen in radiative decay from the $\Upsilon(3S)$ [4]. Masses of the D-wave states have been predicted in potential model calculations (see, for example, [5,6]), but it is hard to quantify the errors in these predictions except by using different forms for the potentials.

In lattice QCD, the starting point is QCD itself. The difficulties with the D-wave states then stem from the signal to noise ratio; the signal falls exponentially in lattice time with the D-wave mass, but the noise falls with the smaller ground-state S-wave mass. Very large samples of meson correlators on full QCD gluon field configurations are then needed to obtain a reliable signal. Here we give the first results from lattice QCD that are able to distinguish the fine structure of D-wave states.

Lattice calculation.—We use ''second-generation'' gluon field configurations recently generated by the MILC Collaboration [7]. These have a gluon action fully improved through $\alpha_s a^2$ [8] and include the effect of u, d, s, and c quarks in the sea using the highly improved staggered quark formalism [9]. The u and d quarks have the same mass m_l, so the configurations are denoted as $n_f = 2+1+1$. We use three ensembles to give two values of the lattice spacing and two values of m_l. The parameters of the ensembles are given in Table I; we label them as 3, 4, and 5 from Ref. [10], in which we mapped out the S- and P-wave bottomonium spectrum and determined the lattice spacing from the Υ ($2S$-$1S$) splitting.

We calculate b quark propagators on these configurations by using an improved lattice discretization of nonrelativistic QCD (NRQCD). NRQCD is an expansion in powers of the heavy quark velocity and therefore good for b quarks since $v^2/c^2 \approx 0.1$ inside their bound states. The Hamiltonian includes all terms through $O(v^4)$ [10]:

$$aH = -\frac{\Delta^{(2)}}{2am_b} - c_1\frac{(\Delta^{(2)})^2}{8(am_b)^3} + c_2\frac{i}{8(am_b)^2}(\nabla\cdot\tilde{\mathbf{E}} - \tilde{\mathbf{E}}\cdot\nabla) - c_3\frac{1}{8(am_b)^2}\sigma\cdot(\tilde{\nabla}\times\tilde{\mathbf{E}} - \tilde{\mathbf{E}}\times\tilde{\nabla}) - c_4\frac{1}{2am_b}\sigma\cdot\tilde{\mathbf{B}} + c_5\frac{\Delta^{(4)}}{24am_b} - c_6\frac{(\Delta^{(2)})^2}{64(am_b)^2}. \quad (1)$$

Here ∇ is the symmetric lattice derivative, and $\Delta^{(n)}$ is the lattice discretization of the continuum $\sum_i D_i^n$. $\tilde{\mathbf{E}}$ and $\tilde{\mathbf{B}}$ are the chromoelectric and chromomagnetic fields, respectively. am_b is the bare b quark mass, which is tuned by determination on the lattice of the spin average of ground-state Υ and η_b meson masses. This was done in Ref. [10] to give the values used here, quoted in Table II.

The v^4 terms in δH have coefficients c_i whose values are fixed from matching lattice NRQCD to full QCD, either perturbatively or nonperturbatively. Here we use coefficients for c_1, c_5, and c_6 that include $O(\alpha_s)$ corrections, as described in Ref. [10]. The coefficients c_3 and c_4 of the spin-dependent v^4 terms have been tuned from a study of the fine structure of the $\chi_b(1P)$ states. We find $c_3 = 1.0$ with an error of 0.1. c_4 is significantly larger. Here we use $c_4 = 1.25$ on the coarse lattices and 1.10 on the fine lattices. These agree within 0.1 both with the value required

TABLE I. Details of the MILC gluon field ensembles used in this Letter. a is the lattice spacing in femtometers determined from the Υ ($2S$-$1S$) splitting, and L/a and T/a give the lattice size. am_l, am_s, and am_c are the sea quark masses in lattice units. Ensembles 3 and 4 are denoted "coarse" and 5 "fine."

Set	a (fm)	am_l	am_s	am_c	$L/a \times T/a$
3	0.1219(9)	0.0102	0.0509	0.635	24×64
4	0.1195(10)	0.005 07	0.0507	0.628	32×64
5	0.0884(6)	0.0074	0.037	0.440	32×96

to give P-wave fine structure, in agreement with experiment, and with the $O(\alpha_s)$ improved result [10].

To make meson correlators for D-wave states, we use a quark propagator made from either a local or a smeared source which has appropriate derivatives applied to it to generate a D "wave function." This propagator is then combined with a local propagator and the same derivatives and smearings applied at the sink to create a 2×2 matrix of correlators for each D-wave state. The complete set of combinations of spin matrices and derivatives needed is given in Ref. [11]. Note that the spin-2 and spin-3 representations split into irreducible representations of the lattice rotational group $\{A_1, A_2, E, T_1, T_2\}$, which must be considered independently since their masses can differ by discretization errors. Very high statistics is required—we have typically 32 000 correlators for every source operator per ensemble, using multiple time sources per configuration. The time sources are binned over for analysis.

TABLE II. Fitted D-wave energies on each ensemble. Errors are from statistics and fitting only. $c_3 = 1.0$ on all ensembles; $c_4 = 1.25$ on sets 3 and 4 and 1.10 on set 5. $a\Delta(x) = aE(x) - aE(^3\bar{D})$. R_X and Δ_X are defined in the text. The A_2 irrep on set 5 is fit separately and not included in the splittings.

	Set 3 $am_b = 2.66$	Set 4 $am_b = 2.62$	Set 5 $am_b = 1.91$
$aE(1\,^1D_{2E})$	0.705(10)	0.694(12)	0.594(5)
$aE(1\,^1D_{2T_2})$	0.711(8)	0.693(10)	0.589(3)
$aE(1\,^3D_{1T_1})$	0.695(7)	0.680(10)	0.575(8)
$aE(1\,^3D_{2E})$	0.698(10)	0.692(10)	0.588(4)
$aE(1\,^3D_{2T_2})$	0.702(8)	0.691(10)	0.589(4)
$aE(1\,^3D_{3A_2})$	0.707(10)	0.704(10)	0.597(4)
$aE(1\,^3D_{3T_1})$	0.715(7)	0.705(8)	0.596(4)
$aE(1\,^3D_{3T_2})$	0.714(7)	0.696(9)	0.594(3)
$a\Delta(1\,^1D_2)$	0.0029(31)	0.0004(37)	0.0027(27)
$a\Delta(1\,^3D_1)$	−0.0104(34)	−0.0137(44)	−0.0137(62)
$a\Delta(1\,^3D_2)$	−0.0047(23)	−0.0021(21)	0.0001(20)
$a\Delta(1\,^3D_3)$	0.0078(22)	0.0074(27)	0.0069(20)
R_D	1.318(23)	1.303(26)	1.309(16)
$a\Delta_{\mathbf{L}\cdot\mathbf{S}}$	0.0038(11)	0.0040(13)	0.0037(13)
$a\Delta_{S_{ij}}$	−0.0005(9)	0.0009(9)	0.0016(15)
$R_{\mathbf{L}\cdot\mathbf{S}}$	0.44(13)	0.49(17)	0.60(21)
$R_{S_{ij}}$	−0.26(52)	0.53(50)	1.1(1.0)

Bayesian fitting [12] is used to extract the spectrum from the correlators by using the fit function:

$$G_{\text{meson}}(n_{sc}, n_{sk}; t) = \sum_{k=1}^{n_{\text{exp}}} a(n_{sc}, k) a^*(n_{sk}, k) e^{-E_k t}. \quad (2)$$

E_k is the energy of the $(k-1)$th radial excitation, and $a(n, k)$ label the amplitudes depending on source and sink smearing. We fit all the D-wave states together, taking the ^3D_2E state as the reference state, with a prior of width 0.1 on its ground-state energy. Relative to that, we take prior value 0 ± 40 MeV on the ground-state energy of the other states. We take priors 0.5 ± 0.5 GeV on radial excitation energies and 0.1 ± 1.0 on amplitudes. We fit correlators from time $t/a = 2$ to 12 except for the local-local correlators which we take from $t/a = 9$ to 12.

Results.—The results from our fits for each D-wave lattice representation on each ensemble are given in Table II. We use $n_{\text{exp}} = 3$ on sets 3 and 4 and $n_{\text{exp}} = 4$ on set 5 since these have the highest posterior probability [12]; values and errors have stabilized at this point and $\chi^2/\text{d.o.f.} < 1$. We also give the ratio $R_D = (1\,^3D_2\text{-}1\bar{S})/(2\,^3S_1\text{-}1\,^3S_1)$, where $1\bar{S}$ is the spin average of Υ and η_b energies from Ref. [10] and $1\,^3D_2$ is the dimension-weighted average of the lattice $^3D_{2E}$ and $^3D_{2T_2}$ results.

R_D is plotted along with similarly defined R_S and R_P from Ref. [10] in Fig. 1. To obtain a physical result for R_D, we fit to the same form used in Ref. [10] for R_S and R_P, allowing for lattice spacing and sea quark mass dependence:

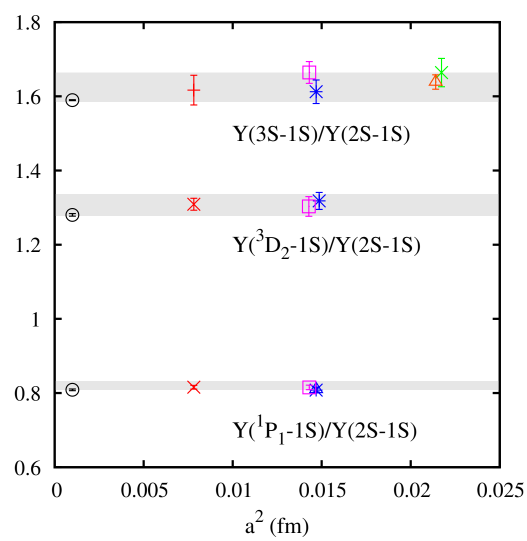

FIG. 1 (color online). Results for the ratio of the 1^3D_2-$1S$ splitting to the $2S$-$1S$ splitting in the Υ system plotted against the square of the lattice spacing determined from the $2S$-$1S$ splitting. Other ratios from Ref. [10] are shown for comparison. The gray shaded bands give the physical result obtained from a fit to the data as described in the text and with the full error of Table III. The black open circles slightly offset from $a = 0$ are from experiment [14].

TABLE III. Complete error budget for R_D in percent. The final error takes account of shifts to the meson masses from effects not included in our lattice QCD calculation. This is discussed for R_S and R_P in Ref. [10], where it is also shown that finite volume and m_b tuning errors are negligible.

	R_D
Statistics and fitting	1.4
a dependence	1.4
m_l dependence	0.5
NRQCD am_b dependence	0.1
NRQCD systematics	1.0
Electromagnetism and η_b annihilation	0.2
Total	2.3%

$$R = R_{\rm phys}\bigg[1 + 2b_l\delta x_l[1 + c_l(a\Lambda)^2] + \sum_{j=1,2} c_j(a\Lambda)^{2j}[1 + c_{jb}\delta x_m + c_{jbb}(\delta x_m)^2)\,]\bigg]. \quad (3)$$

Here δx_l is $(am_l/am_s) - (m_l/m_s)_{\rm phys}$ for each ensemble. $(m_l/m_s)_{\rm phys}$ is taken from lattice QCD as 27.2 (3) [13]. $\delta x_m = (am_b - 2.65)/1.5$ allows for am_b effects from NRQCD in the discretization errors over our range of a values. Λ, taken as 500 MeV, sets the scale for physical a dependence. Fit priors are as in Ref. [10]: 1.0 (0.5) on $R_{\rm phys}$; 0.0 (0.3) on a^2 terms; 0.0 (1.0) on higher order in a; 0.0 (0.015) on b_l. The physical result we obtain for R_D is 1.307 (30), after adding an additional NRQCD systematic error for missing v^6 terms [10]. This is to be compared to the experimental value of 1.280 (3). A complete error budget for R_D is given in Table III.

In Fig. 2, we plot the masses of all the lattice representations relative to the spin average of all $1\,^3D$ states for coarse set 4, by using the $2S$-$1S$ splitting to set the scale (Table I). We see that the lattice representations for each spin agree well with each other within our sizable statistical errors. The hyperfine splitting between the $^1D_2$ and the spin average of ^3D states is expected to be very small, following results for P-wave states. We find it to be zero to within 10 MeV.

Figure 3 shows the results from all three sets, using a dimension-weighted average of results, including the correlations from the fit, for the different lattice representations for the $^3D_3$ and $^{(1,3)}D_2$. Results are consistent between the fine and coarse sets and between different sea light quark masses for the two coarse sets.

To arrive at a final result for D-wave fine structure, we study combinations of ^3D spin splittings that are sensitive either to an $\mathbf{L}\cdot\mathbf{S}$ or to a tensor S_{ij} interaction ($\mathbf{S}\cdot\mathbf{S}$ takes the same value for all ^3D states). Writing

$$M_J = \bar{M}(^3D) + \Delta^D_{\mathbf{L}\cdot\mathbf{S}}\langle \boldsymbol{L}\cdot\boldsymbol{S}\rangle + \Delta^D_{S_{ij}}\langle S_{ij}\rangle \quad (4)$$

gives

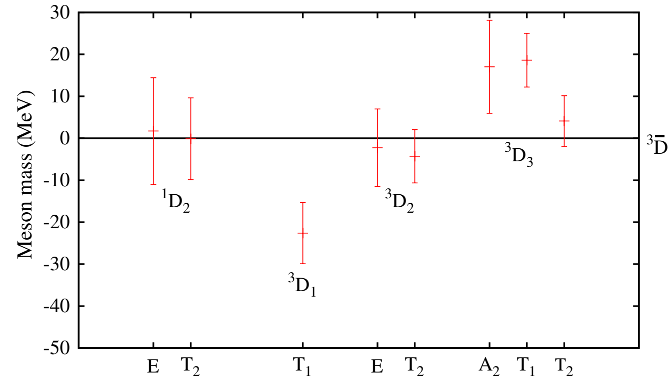

FIG. 2 (color online). Results for the separate irreducible representations of the lattice rotation group making up each continuum D-wave state on coarse set 4. Statistical errors vary with the dimension of the representation. For the $^3D_3$, we have dimensions A_2, 1; T_1, 3; T_2, 3.

$$\Delta^D_{\mathbf{L}\cdot\mathbf{S}} = (14M_3 - 5M_2 - 9M_1)/60,$$
$$\Delta^D_{S_{ij}} = -7(2M_3 - 5M_2 + 3M_1)/120. \quad (5)$$

Table II gives our results for these splittings. In Fig. 4, we plot ratios to the equivalent ^3P splitting combinations: $R_X = \Delta^D_X/\Delta^P_X$ with $\Delta^P_{\mathbf{L}\cdot\mathbf{S}} = (5M_2 - 3M_1 - 2M_0)/12$ and $\Delta^P_{S_{ij}} = -5(M_2 - 3M_1 + 2M_0)/72$. Values for Δ^P for these ensembles are given in Ref. [10] (without factors of 1/12 and $-5/72$). The experimental values are $\Delta^P_{\mathbf{L}\cdot\mathbf{S}} =$ 13.65(27) MeV and $\Delta^P_{S_{ij}} = 3.29(9)$ MeV [14]. The advantage of using these combinations is that they depend purely on one of the spin-dependent coefficients of the NRQCD action. On set 5 we did not use exactly the same values for c_3 and c_4 in our study of P and D waves. However, we can correct for this in Fig. 4, since $\Delta_{S_{ij}} \propto c_4^2$ and $\Delta_{\mathbf{L}\cdot\mathbf{S}} \propto c_3$.

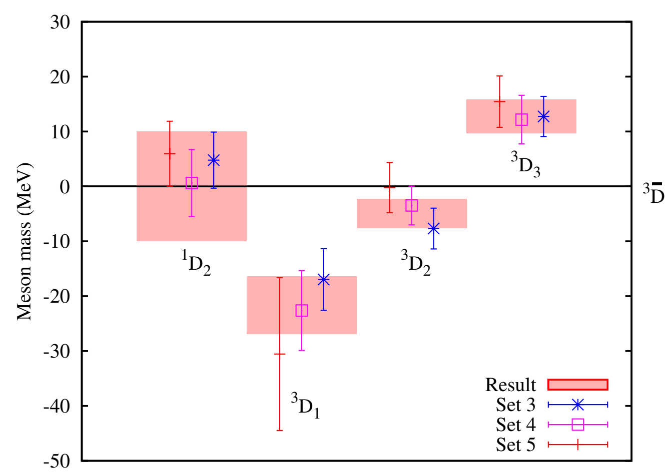

FIG. 3 (color online). D-wave masses plotted relative to the ^3D spin average for all sets using the $2S$-$1S$ splitting to set the scale. The red shaded bands show our final results using ratios of combinations of splittings to those of P-wave states as described in the text.

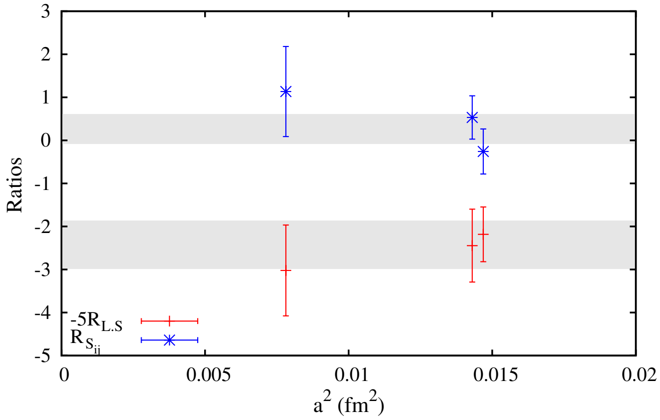

FIG. 4 (color online). Ratios $R_{S_{ij}}$ and $R_{\mathbf{L}\cdot\mathbf{S}}$ (multiplied by -5 for clarity) plotted against the square of the lattice spacing. The gray bands give our physical results.

Once this slight adjustment is done, the dependence on $c_{3,4}$ cancels between P and D states, and so errors from the uncertainty in these coefficients are much reduced.

We fit the fine-structure R values to the same form used earlier in Eq. (4) to extract physical results:

$$R_{\mathbf{L}\cdot\mathbf{S}} = 0.49\,(11); \qquad R_{S_{ij}} = 0.26\,(35). \tag{6}$$

We have included an additional systematic error of 10% to allow for missing v^6 terms from our NRQCD action, but the lattice statistical error dominates. We then combine the R values with experimental results from $1P$ levels to give the following ^3D splittings:

$$\begin{aligned} {}^3D_3 - {}^3D_1 &= 34(8)\ \text{MeV}, \\ {}^3D_3 - {}^3D_2 &= 18(5)\ \text{MeV}, \\ {}^3D_2 - {}^3D_1 &= 17(6)\ \text{MeV}. \end{aligned} \tag{7}$$

Our fine-structure splittings are somewhat larger than typical results from potential models [5,6], where the $^3D_3 - {}^3D_1$ splitting lies in the range 10–20 MeV. This can be traced to a larger value for $R_{\mathbf{L}\cdot\mathbf{S}}$ than is obtained, for example, in Ref. [5], based on specific forms for the spin-dependent potentials.

One issue that we have neglected above is that the $^3D_1$ state has $J^{PC} = 1^{--}$ in common with $^3S_1$ states. On the lattice, in principle, any operator with 1^{--} quantum numbers will be able to create all 1^{--} states. In practice, the amplitude for $^3S_1$ states to be created by the operators that we use for the $^3D_1$ is very small and vice versa. We illustrate that in Fig. 5, where we show correlators from set 3 that use a local $^3S_1$ or $^3D_1$ operator at source and sink compared to the cross correlator that has a local $^3S_1$ operator at the source and $^3D_1$ at sink or vice versa. The cross correlator is much smaller in magnitude than either of the diagonal correlators at small t values. The exponential falloff (as seen in the slope of the log plot) of the cross correlator matches that of the $^3S_1$ correlator at large times,

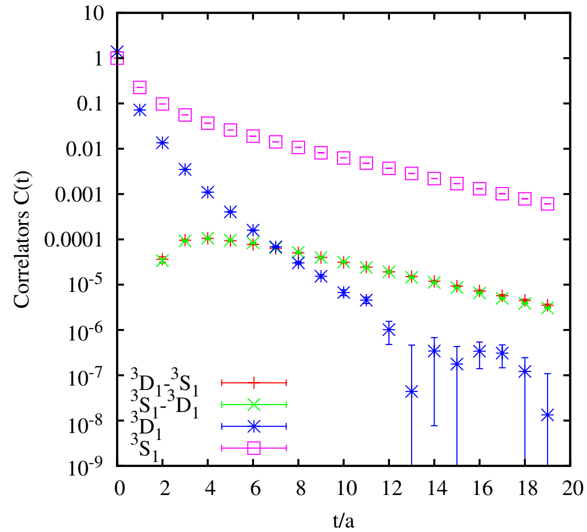

FIG. 5 (color online). Correlators made from different combinations of local $^3S_1$ and $^3D_1$ operators at source and sink, plotted with a logarithmic y axis as a function of lattice time t. Results are from set 3.

where the $^3D_1$ correlator falloff is dominated by that of the heavier $^3D_1$ state. If we fit the complete set of $^3S_1$ and $^3D_1$ correlators together, including the local cross correlators of Fig. 5, we obtain results in agreement with our separate fits for $^3S_1$ (in Ref. [10]) and $^3D_1$ masses. We also find, for example, that the amplitude $a(^3D_{1,\text{local}}, \Upsilon)$ from Eq. (2) is 0.0052(1) times that of $a(^3S_{1,\text{local}}, \Upsilon)$.

Conclusions.—We give the first full lattice QCD results for the D-wave states of bottomonium including the fine structure. We obtain a mass of 10.179(17) GeV for the $1\,^3D_2$ to be compared with 10.1637(14) GeV from experiment [14]. Using the experimental result for the $1\,^3D_2$ mass, we predict masses of 10.181(5) GeV for the $1\,^3D_3$, 10.147(6) GeV for the $1\,^3D_1$, and 10.169(10) GeV for the $^1D_2$.

We are grateful to the MILC Collaboration for the use of their gauge configurations and to Peter Lepage for comments. We used the Darwin Supercomputer under the DiRAC facility jointly funded by STFC, BIS, and the Universities of Cambridge and Glasgow. This work was funded by STFC and the EU Erasmus program.

*Present address: HISKP, Universität Bonn, 53115 Bonn, Germany.
†c.davies@physics.gla.ac.uk
‡Rachel.Dowdall@glasgow.ac.uk
§http://www.physics.gla.ac.uk/HPQCD

[1] B. Aubert *et al.* (*BABAR* Collaboration), Phys. Rev. Lett. **101**, 071801 (2008).
[2] I. Adachi *et al.* (Belle Collaboration), arXiv:1103.3419.
[3] A. Gray *et al.* (HPQCD Collaboration), Phys. Rev. D **72**, 094507 (2005).

[4] G. Bonvicini *et al.* (CLEO Collaboration), Phys. Rev. D **70**, 032001 (2004).
[5] W. Kwong and J. L. Rosner, Phys. Rev. D **38**, 279 (1988).
[6] N. Brambilla *et al.* (Quarkonium Working Group), arXiv:hep-ph/0412158.
[7] A. Bazavov *et al.* (MILC Collaboration), Phys. Rev. D **82**, 074501 (2010).
[8] A. Hart, G. M. von Hippel, and R. R. Horgan (HPQCD Collaboration), Phys. Rev. D **79**, 074008 (2009).
[9] E. Follana *et al.* (HPQCD Collaboration), Phys. Rev. D **75**, 054502 (2007).
[10] R. J. Dowdall *et al.* (HPQCD Collaboration), arXiv:1110.6887 [Phys. Rev. D (to be published)].
[11] C. T. H. Davies *et al.*, Phys. Rev. D **50**, 6963 (1994).
[12] G. P. Lepage *et al.*, Nucl. Phys. B, Proc. Suppl. **106**, 12 (2002).
[13] A. Bazavov *et al.*, Rev. Mod. Phys. **82**, 1349 (2010).
[14] K. Nakamura *et al.* (Particle Data Group), J. Phys. G **37**, 075021 (2010).